IEEE Access
Multidisciplinary ⋮ Rapid Review ⋮ Open Access Journal

Received 24 November 2022, accepted 11 January 2023, date of publication 31 January 2023, date of current version 3 February 2023.

Digital Object Identifier 10.1109/ACCESS.2023.3241067

RESEARCH ARTICLE

A Study on Design Method of Synchronous Reluctance Motor Based on Nonlinear MEC Using Newton-Raphson Method

DONG-HOON JUNG[1], KI-DEOK LEE[2], AND JAE-KWANG LEE[2]

[1]School of Mechanical, Automotive and Robot Engineering, Halla University, Wonju 26404, South Korea
[2]Intelligent Mechatronics Research Center, Korea Electronics Technology Institute, Bucheon 14502, South Korea

Corresponding author: Jae-Kwang Lee (leejk@keti.re.kr)

This work was supported by the National Research Foundation of Korea (NRF) Grant through the Korea Government (MSIT) under Grant 2020R1F1A1075209.

ABSTRACT Recently, policies for carbon reduction are being implemented worldwide to solve environmental and energy consumption problems. Minimum Energy Performance Standard (MEPS) is a carbon reduction policy for reducing energy consumption by regulating the efficiency of industrial induction motors. The induction motors have a low manufacturing cost and a simple structure, and it can be operated without control and have great advantages in maintenance so it is applied in various industrial fields. However, compared with other types of motors, there is a limit to improving the efficiency due to the additional loss generated in the cage of rotor. Synchronous reluctance motors (SynRMs) are attracting the most attention as an alternative to an induction motor since they are composed of only a copper winding and a core, manufacturing cost and durability are excellent Moreover, unlike induction motors, there is no secondary loss; therefore, it is evaluated as a high-efficiency industrial motor corresponding to MEPS. However, because of their complex rotor shape composed of multiple barriers and segments, SynRMs are typically designed using finite-element analysis, requiring a significant amount of time and trial and error. In this paper, a basic design method for a synchronous reluctance motor based on a nonlinear magnetic equivalent circuit using the Newton-Rapson method is presented. Finally, the design method of the synchronous reluctance motor is validated through performance tests using a prototype.

INDEX TERMS Minimum energy performance standard (MEPS), nonlinear magnetic equivalent circuit (MEC), Newton-Raphson method, synchronous reluctance motor (SynRM).

I. INTRODUCTION

Electricity consumption is rapidly increasing owing to the electrification of industries and convenience of electrical energy. Therefore, energy consumption regulations and high-efficiency policies are being implemented worldwide to reduce the energy consumption. The Minimum Energy Performance Standard (MEPS) is a policy for reducing the electrical energy consumption. It classifies the efficiency of induction motors, which account for a large portion of electricity consumption, into five levels and restricts the use of induction motors that are less than the national standard efficiency [1], [2], [3]. The induction motor has a simple shape and low material price; therefore it is easy to manufacture and has excellent price competitiveness compared with other motors. However, there is a limit to efficiency improvement owing to the secondary loss occurring in the squirrel cage bar of its rotor. To improve the efficiency of induction motors from IE3 (High efficiency) to IE4 (Super premium efficiency) of MEPS, research and development of efficiency improvement of the induction motors is being actively conducted [4], [5]. But this is insufficient because of the price increase due to the material change of the squirrel cage bar for reduction the secondary loss and the technical limitations of die casting. The synchronous reluctance motor (SynRM) is a non-rare earth motor, and its rotor is composed

The associate editor coordinating the review of this manuscript and approving it for publication was Montserrat Rivas.

of barriers, composed of air, and an iron core. It generates reluctance torque using the d-q axis inductance difference generated by the shape of the segment. Besides, the SynRM is composed of an iron core and copper windings; therefore, its structure and manufacturing process are simpler than those of an induction motor. Moreover, unlike induction motors, secondary loss does not occur; therefore, as an industrial motor, it can secure IE4 or higher efficiency by replacing induction motors. However, the rotor of a SynRM has a complex shape composed of multiple barriers and segments, so finite element analysis (FEA) is required for such complex shape design and characteristic analysis, which takes a lot of time and trial and error [6], [7], [8]. In this study, a basic design method for a SynRM based on a nonlinear magnetic equivalent circuit (MEC) using the Newton-Raphson method is presented. When the design method proposed in this paper is applied for designing the SynRM, it may differ from the design and analysis conditions of the FEA; however, it reduces the time and number of analyses to derive the basic model. Additionally, rotor optimal design was performed using the output characteristic maps according to the main design variables of the rotor, and its structural stability during rotation was verified through structural analysis. Finally, the validity of the design method for a SynRM using the nonlinear MEC was verified through FEA and performance tests with a prototype.

II. DESIGN PROCESS OF SYNCHRONOUS RELUCTANCE MOTOR

A SynRM was designed in the order of the basic design based on a nonlinear MEC using the Newton-Raphson method and the optimal design of the rotor using the output characteristic map according to the main design variables of the rotor, as shown in Fig. 1. After calculating the torque for the unit stack length (1 mm) of the motor through a nonlinear MEC, the stack length was calculated to satisfy the required torque. Thereafter, the output characteristics (torque, loss, efficiency, and THD) were reviewed using an output characteristic map according to the main design variables of the rotor, and the final model was derived by performing an optimal design based on the results of the review.

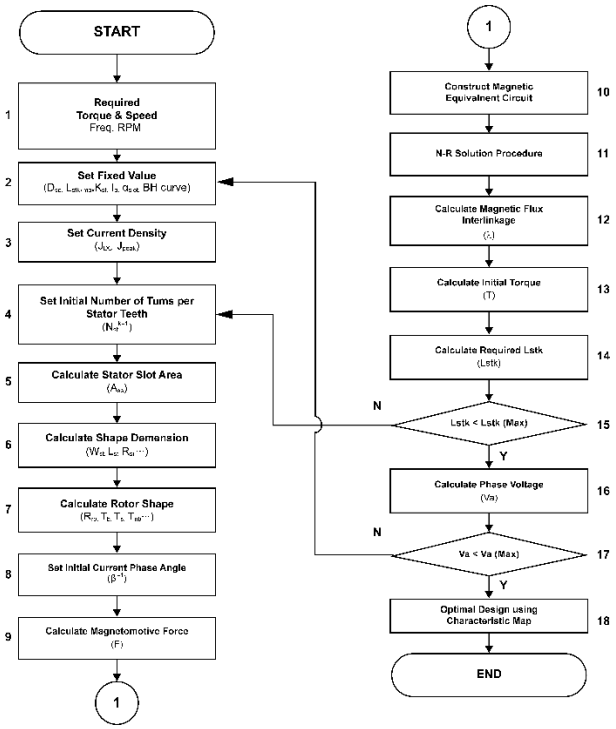

FIGURE 1. Design process of SynRM.

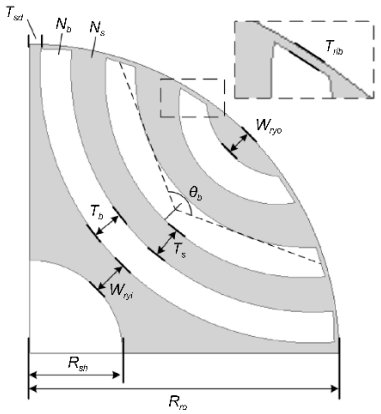

FIGURE 2. Design variables of the rotor with arc-type barriers.

III. DESIGN OF SYNCHRONOUS RELUCTANCE MOTOR BASED ON THE NONLINEAR MEC

Mathematical modeling of the stator and rotor is required to calculate the magnetoresistance of each element for designing the magnetic equivalent circuit of the motor. The SynRM uses the reluctance torque generated by the d-q-axi inductance difference of the rotor, expressed in (1), so the rotor is composed of numerous design variables [7], [9], [10]. Therefore, among the stator and rotor of the motor, this study focuses on the mathematical modeling method of the SynRM rotor, which has a more complex shape than other motors.

$$T = \frac{3}{2}p(\lambda_d i_q - \lambda_q i_q) = \frac{3}{2}p((L_d - L_q)i_q i_d)\ [Nm] \quad (1)$$

where λ_{dq} is the d-q axis flux linkage, i_{dq} is the d-q axis current, and p is the number of pole pairs.

A. MATHEMATICAL MODELING OF THE ROTOR

SynRM in this paper has arc-type barriers as shown in Fig. 2, and a total of 11 design variables for mathematical modeling of the rotor are set as shown in Table 1. Among the design variables, the thickness of each barrier and segment (T_{b1} ~T_{bn}, T_{s1} ~T_{sn}) was designated as No. 1 from the inside, T_{sd} is the thickness between the first barrier and the d-axis.

For barrier shape design, eight points were set on the barrier as shown in Fig. 2, where θ_a given by (2) is the angle of the barrier end (P_1) from the origin (P_o), and the barrier angle

TABLE 1. Design variables of the Rotor.

Number	Variables	Symbol
1	Number of Barrier	N_b
2	Number of Segment	N_{seg}
3	Radius of Rotor	R_{ro}
4	Radius of Shaft	R_{sh}
5	Thickness of Barrier	$T_{b1\sim bn}$
6	Thickness of Segment	$T_{s1\sim sn}$
7	Thickness of Segment(d-axis~T_{b1})	T_{sd}
8	Width of Inner yoke	W_{ryi}
9	Width of Outer yoke	W_{ryo}
10	Thickness of Rib	T_{rib}
11	Angle of Barrier	θ_b

(θ_b) can be calculated using the variables listed in Table 1.

$$\theta_a = \sin^{-1}\left(\frac{T_{sd}}{R_{ro}-T_{rib}}\right)$$
$$\theta_b = 2\tan^{-1}\left(\frac{(R_{ro}-T_{rib})\sin(\pi/4-\theta_a)}{(R_{ro}-T_{rib})\cos(\pi/4-\theta_a)-R_{sh}-W_{ry}}\right) \quad (2)$$

Pos_{b1} is the position of the barrier, indicating its position from the origin to the center of the barrier. k_{b1} is a variable used to obtain the angle of the barrier with respect to the origin; θ_{ob1} can be derived using the variable in (3). Using the position and angle of the barrier from (3), eight points constituting the barrier can be calculated and the shape of the barrier can be designed using each point.

$$\begin{aligned} Pos_{b1} &= R_{sh}+W_{ryi}+T_{b1}/2 \\ k_{b1} &= Pos_{b1}\cos(\theta_b/2) \\ &\quad +\sqrt{(Pos_{b1}\cos(\theta_b/2))^2+(R_{ro}-T_{rib})^2-Pos_{b1}^2} \\ \theta_{ob1} &= \sin^{-1}\left(\frac{k_{b1}\sin(\theta_b/2)}{R_{ro}-T_{rib}}\right) \end{aligned} \quad (3)$$

Based on P_1, the width of the barrier used to calculate the magnetic resistance of the rotor was calculated using (4).

The variables of the remaining barriers were calculated using the relative relationships with variables of the first barrier.

$$\begin{aligned} P_1 &= (X_{b1}, Y_{b1}) \\ X_{b1} &= (R_{ro}-T_{rib})\cos(\theta_{ob1}+\pi/4) \\ Y_{b1} &= (R_{ro}-T_{rib})\sin(\theta_{ob1}+\pi/4) \\ l'_{b1} &= \sqrt{2\left(\frac{2(Pos_{b1}\cos(\pi/4))^2-X_{b1}^2-Y_{b1}^2}{4Pos_{b1}\cos(\pi/4)-2X_{b1}-2Y_{b1}}\right)^2} \\ R_{b1} &= l'_{b1}-Pos_{b1} \\ W_{b1} &= 2R_{b1}(\pi-\theta_b) \end{aligned} \quad (4)$$

The variables for the segment can also be calculated in the same way as the variables of the barrier obtained above. However, if it is assumed that the magnetic path of the segment is orthogonal to the barrier, the width of the derived barrier is converted into the length of the magnetic path of the segment.

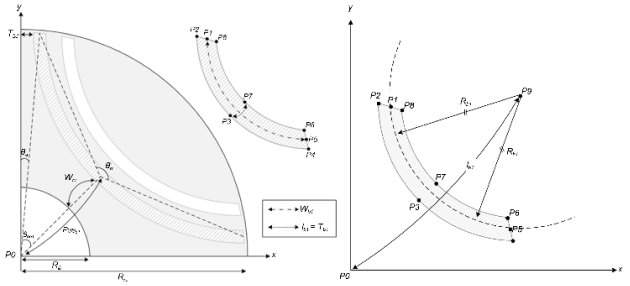

FIGURE 3. Specific design variables of the arc-type barriers.

B. DESIGN OF NONLINEAR MEC FOR SynRM

When current is applied to the SynRM (under load), the magnetic flux density distribution of the rotor can be divided into segments, barriers, and ribs. Additionally, the magnetic flux saturation level of each segment and the leakage flux to the barrier changed according to the number of segments and barriers. Therefore, using the rotor shape variables calculated above, the magnetic resistance of the barrier and the segment should be calculated according to the number of each elements as in (5). Further, the magnetic resistance of the rib can be calculated from the thickness and length of the rib using (6). Here, the length of the magnetic path was the same as the thickness of the barrier.

$$\begin{aligned} \Re_{seg} &= \frac{l_{sn}/n_s}{\mu_0\mu_{core}A_{sn}} = \frac{l_{sn}/n_s}{\mu_0\mu_{core}W_{sn}L_{stk}} = \frac{l_{sn}/n_s}{\mu_0\mu_{core}T_{sn}L_{stk}} \\ \Re_b &= \frac{l_{bn}}{\mu_0 A_{bn}} = \frac{l_{bn}}{\mu_0(W_{bn}/n_b)L_{stk}} = \frac{T_{bn}}{\mu_0(W_{bn}/n_b)L_{stk}} \end{aligned} \quad (5)$$

$$\Re_{rr} = \frac{l_{rib}}{\mu_0\mu_{core}A_{rib}} = \frac{l_{rib}}{\mu_0\mu_{core}W_{rib}L_{stk}} = \frac{T_b}{\mu_0\mu_{core}T_{rib}L_{stk}} \quad (6)$$

Here, l_{sn} is the nth segment length, $\mathbf{l}_{sb}$ is the nth barrier length, l_{rib} is the rib length, n_s is the number of divisions in segment length, n_b is the number of divisions of barrier area.

Using the magnetic resistance of the rotor elements calculated above and the magnetomotive force, the magnetic equivalent circuit of SynRM consisting of the rotor with the segments and barriers and the stator can be designed as shown in Fig. 4. The matrix of magnetomotive force can be calculated from (7) by applying Kirchhoff's Voltage Law (KVL) to each MEC closed circuit.

$$\boldsymbol{A}_R\boldsymbol{\varphi} = \boldsymbol{F} \quad (7)$$

Here, $\mathbf{A}_R$ is the Symmetric matrix of magnetic resistance, $\boldsymbol{\varphi}$ is the matrix of magnetic fluxes in the closed-loop, and $\mathbf{F}$ is the matrix of magnetomotive force.

The electrical steel sheet applied to the core of the motor has nonlinear magnetic saturation characteristics. Particularly, because the rotor of the SynRM is composed of a number of segments made of cores, a design that reflects the nonlinear characteristics of electrical steel sheets is essential.

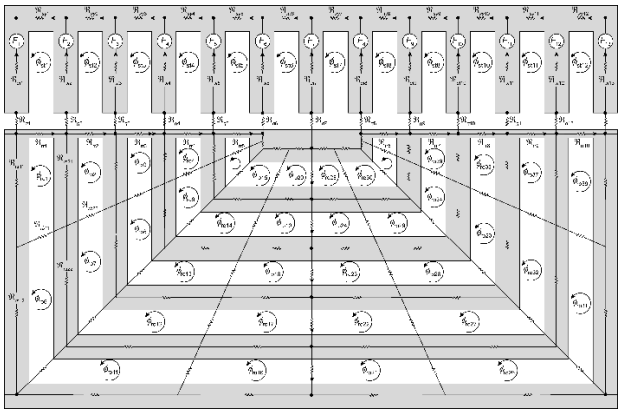

FIGURE 4. Magnetic equivalent circuit of SynRM.

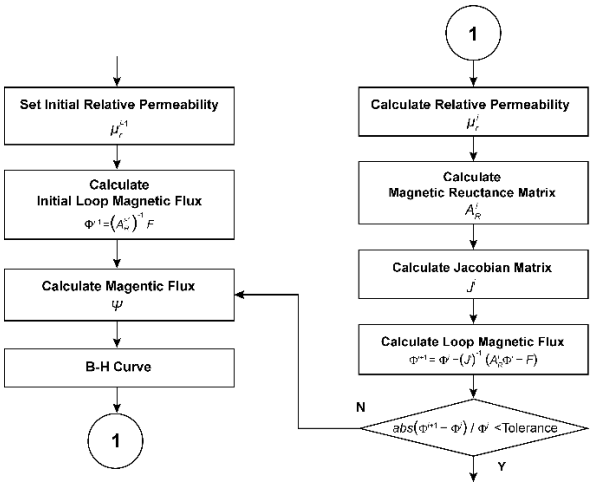

FIGURE 5. Process of the nonlinear analysis using Newton-Raphson method.

After making (7) as (8) in order to consider the nonlinear characteristics of the core, the magnetic flux matrix can be obtained as shown in (9) using the Newton-Raphson method.

$$\begin{aligned} \boldsymbol{g}(\boldsymbol{\varphi}) &= \boldsymbol{A}_R\boldsymbol{\varphi} - \boldsymbol{F} = \boldsymbol{0} \\ &= [g_1(\boldsymbol{\varphi}), g_2(\boldsymbol{\varphi}), \cdots g_n(\boldsymbol{\varphi})]^T \quad (8) \\ \boldsymbol{\varphi}_{i+1} &= \boldsymbol{\varphi}_i - \boldsymbol{J}^{-1}\boldsymbol{g}(\boldsymbol{\varphi}_i) \quad (9) \end{aligned}$$

Here, $\boldsymbol{J}$ is a Jacobian matrix defined as a first-order differential matrix for a multivariate vector function, expressed as (10). which can be calculated as in (11) by generalizing using the magnetic resistance matrix ($\mathbf{A}_R$).

$$\boldsymbol{J} = \begin{bmatrix} \frac{\partial g_1}{\partial \phi_{st1}} & \cdots & \frac{\partial g_1}{\partial \phi_{ronr}} \\ \vdots & \ddots & \vdots \\ \frac{\partial g_n}{\partial \phi_{st1}} & \cdots & \frac{\partial g_n}{\partial \phi_{ronr}} \end{bmatrix} \quad (10)$$

$$\boldsymbol{J} = \boldsymbol{A}_R + \boldsymbol{p}\boldsymbol{A}_R \quad (11)$$

Here, $\boldsymbol{pA}_\mathrm{R}$ is the product of the derivative of the magnetic resistance of $\boldsymbol{A}_\mathrm{R}$ by the closed-loop magnetic flux and the closed-loop magnetic flux [11], [12].

The nonlinear analysis process based on the Newton-Raphson method using the design variables and matrices for nonlinear analysis calculated so far is shown in Fig. 5. The initial closed-loop magnetic flux was calculated by assuming the initial permeability. The magnetic flux flowing through the magnetic resistance was calculated using the calculated initial closed-loop magnetic flux, and the magnetic permeability of the electrical steel sheet was recalculated using the B-H curve. The matrices of $\boldsymbol{A}_\mathrm{R}$ and $\boldsymbol{J}$ were calculated using the recalculated permeability, and the closed-loop magnetic flux was calculated using these matrices. Nonlinear analysis was performed by repeating this process till it reached the allowable error range by calculating the difference from the previously calculated closed-loop magnetic flux. Using the magnetic flux derived through the nonlinear analysis, the magnetic flux matrix flowing through the stator teeth was derived and multiplied by the number of turns to calculate the three-phase armature flux linkage, expressed in (12). The torque and inductance of (1) can then be calculated through the dq-axis coordinate transformation of the flux linkage.

TABLE 2. Specifications and constraints of design.

Contents	Value	Unit
Power	5.5	kW
Torque @ Rated seed	29.2@1,800	Nm@rpm
Limit of Voltage	280	$V_{ph,1st}$
THD	10	%
Diameter of Stator	228	mm
Stack Length	140	mm

$$\begin{aligned} \boldsymbol{\Phi}_{st} &= [\Phi_{st1}, \Phi_{st2}, \Phi_{st3}, \cdots, \Phi_{st22}, \Phi_{st23}, \Phi_{stn}]^T \\ \boldsymbol{\lambda}_{abc} &= \boldsymbol{N}_{st}^T\boldsymbol{\Phi}_{st} \quad (12) \end{aligned}$$

C. BASIC DESIGN OF SynRM USING THE NONLINEAR MEC

The synchronous reluctance motor designed in this paper is intended to replace the 5.5kW induction motor, and the load characteristics and design constraints are the same as those of the existing induction motor. The existing induction motor has 4 poles, and the driving speed is 1800rpm (60Hz), and the torque at the rated speed to satisfy the required output is 29.2Nm. From this, the design specifications and constraints of SynRM were determined as shown in Table 2. Fig. 6 shows the design results derived through the nonlinear MEC.

The solid line in Fig. 6(a) represents the torque calculated for an initial stacking length of 1 mm, and the bar graph shows the stacking length required for each number of turns required to satisfy the output. Fig. 6(b) shows the output power and efficiency of each model when designed with the required stacking length in (a). A basic SynRM model was designed using the results of nonlinear MEC. To confirm its validity, the design results were compared with those of FEA. Table 3 shows the comparison with the FEA results;

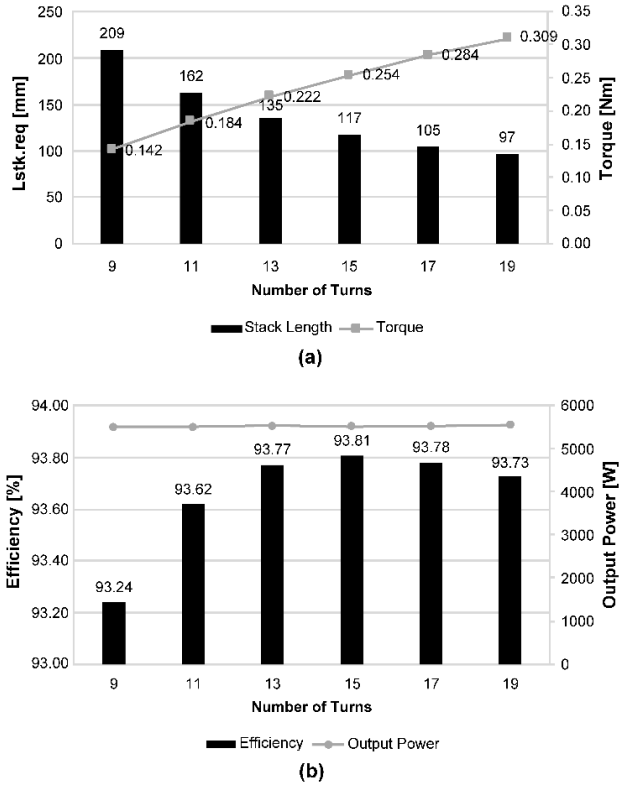

FIGURE 6. Design results using the nonlinear MEC for 5.5kW SynRM (a) torque and required stack length (b) power and efficiency.

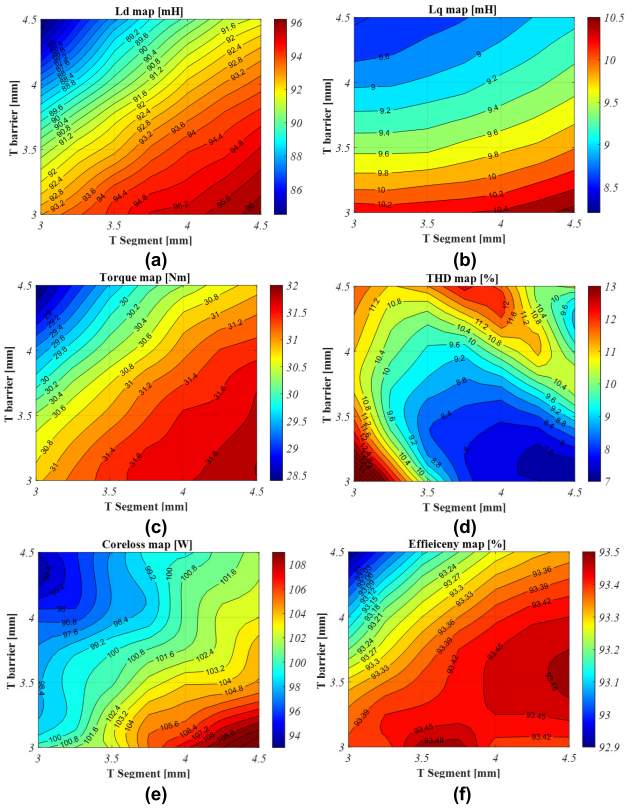

FIGURE 7. Output characteristic maps by the thickness of the barrier and segment (a) d-axis inductance (b) q-axis inductance (c) torque (d) THD (e) coreless (f) efficiency.

TABLE 3. Comparison of MEC and FEA.

Contents	MEC	FEA	Unit
Input Current	12		A
Current phase angle	60		degE
d-axis inductance	84.5	84.5	mH
q-axis inductance	6.4	8	mH
Torque	29.2	28.5	Nm
Error	2.5		%

the torque error between the two results was 2.5% under the same input current and current phase angle. Thus, the basic design of the SynRM using nonlinear MEC is valid.

D. OPTIMAL DESIGN OF SynRM AND STRUCTURAL ANALYSIS

The rotor of SynRM is composed of multiple variables, so it is necessary to review the output characteristics according to the main design variables and to carry out an optimal design based on them in order to satisfy and improve additional required output characteristics after the basic design. Among the diverse design variables, the thicknesses of the barrier and segment have a significant influence on the output characteristics. Therefore, output characteristic maps were derived using the parametric analysis and interpolation method for the barrier and segment thicknesses, and the optimal thickness of the barrier and segment was obtained.

Considering the manufacturability and the effectiveness of output characteristics within the given design constraints, the analysis range for the thickness of the barrier and segment was selected to be 3-4.5 mm, and the output characteristic maps are shown in Fig 7. As a result of the output characteristics maps, the d-axis inductance is proportional to the thickness of segment which is the d-axis magnetic path as shown in Fig. 8 and inversely proportional to the barrier thickness. On the other hand, the q-axis inductance is inversely proportional to the thickness of the barrier. Since the reluctance torque is generated by the difference in the d-q axis inductance as shown in (1), it can be confirmed that the difference in the d-q-axis inductance according to the thickness of the barrier and the segment coincides with the torque trend. However, because the core loss increases with increasing segment thickness, the point of maximum efficiency differs from that of maximum torque. Therefore, based on the optimal design using the output characteristic map, the thicknesses of the barrier and segment were designed to be 3.5 and 4.5 mm, respectively, to obtain maximum efficiency within the design range that satisfies the required torque, and THD satisfies the design constraints. To further improve the output characteristics (maximizing the inductance difference between the d-q axes), an additional barrier was added to the outermost

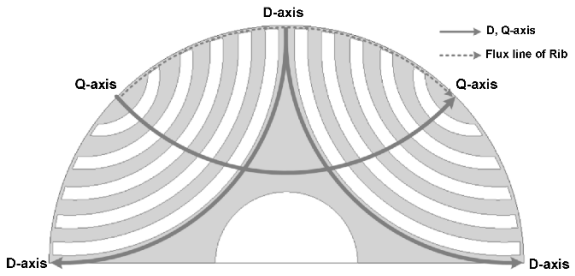

FIGURE 8. D-q axis(Magnetic path) of SynRM.

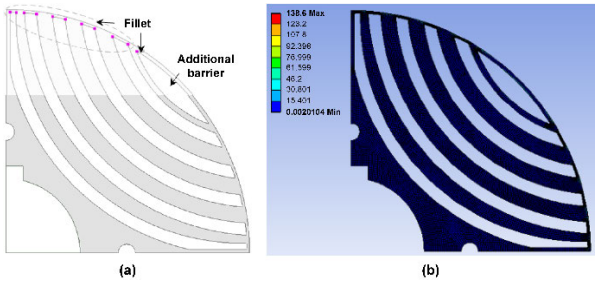

FIGURE 9. Structural analysis of the rotor (a) final model of rotor (b) result of structural analysis.

part of the rotor to derive the final rotor model as shown in Fig. 9(a). The rotor has a rib structure on the outermost part of the rotor to prevent the segment from scattering during rotation as shown in Fig. 8. When the rib structure is applied to the rotor, structural safety can be secured during rotation, but it becomes a part of the q-axis magnetic path to increase the q-axis inductance and decrease the torque. Therefore, after designing the thickness of rib as the minimum thickness within the range that can secure structural safety, the stress was dispersed by applying a fillet to the edge of the barrier where stress is concentrated as shown in Fig. 9 (a). As a result of structural analysis at 2160rpm, which is 20% or more of the rated speed of 1800rpm, for the finally designed rotor, it was confirmed that the maximum stress was 138.6Mpa as shown in Figure 9 (b). The yield strength of the core applied to the rotor is 265Mpa, and as a result of calculating the structural safety factor using (13), it can be confirmed that the target safety factor of 1.7 is satisfied as 1.92.

$$k_{safe} = \frac{\text{Yield Strength}}{\text{Equivalent Stress(Max)}} \tag{13}$$

E. OUTPUT CHARACTERISTICS OF THE FINAL MODEL AND PERFORMANCE TEST USING A PROTOTYPE

The final model of 5.5kW SynRM was derived as shown in Fig. 10 (a). Additionally, Fig. 10 (b) shows the magnetic flux lines and density distribution of the stator and rotor at rated operating. As can be seen from the figure, the magnetic flux density was designed to be less than 1.8T, which is the saturation level of the magnetic flux density of the core applied to the motor. Fig. 11 shows torque and induced voltage when current is applied (under load). Through this, it can be confirmed that the required output is satisfied within

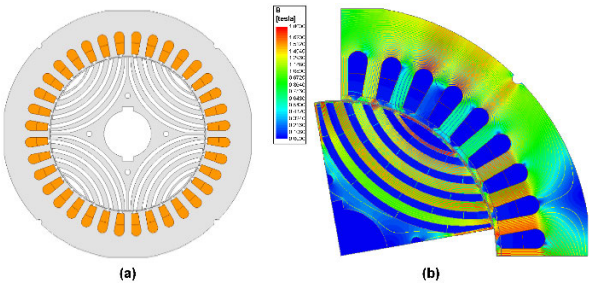

FIGURE 10. Final model of 5.5kW SynRM (a) Final model (b) Magnetic flux lines and density distribution.

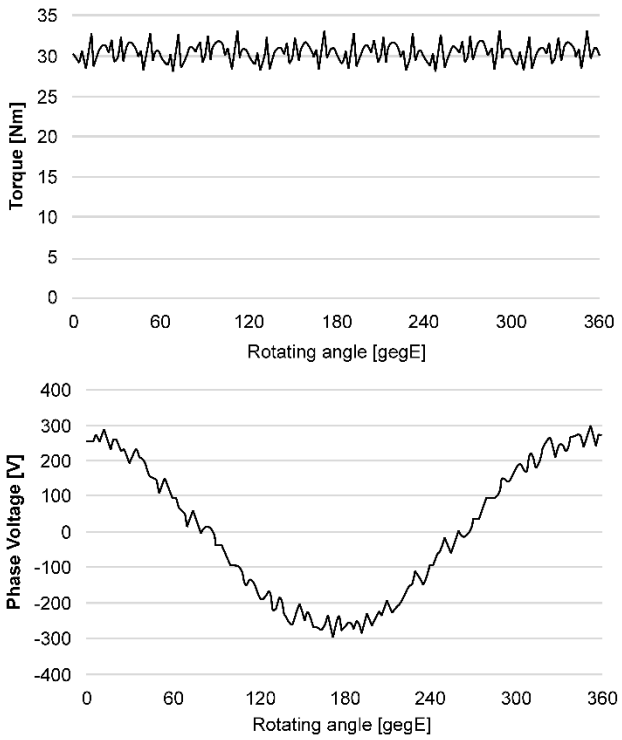

FIGURE 11. Torque and Induced voltage under load.

TABLE 4. Comparison of FEA and performance test.

Contents	FEA	TEST	Unit
Rotating speed	1,800		rpm
Input Current	12.8	13.6	A
Current phase angle	60		degE
Torque	29.3	29.2	Nm
Power	5.53	5.5	kW
Efficiency	95.1	94.7	%

the design constraints. Finally, a performance test using a prototype was conducted to verify the validity of the SynRM design and characteristic analysis results based on the nonlinear MEC and FEA. Fig. 12 shows the test environment composed of the dynamo system for the load test.

Table 4 shows the comparison of FEA and performance test results for the final model of 5.5kW SynRM. From the FEA and performance test, it was confirmed that the SynRM

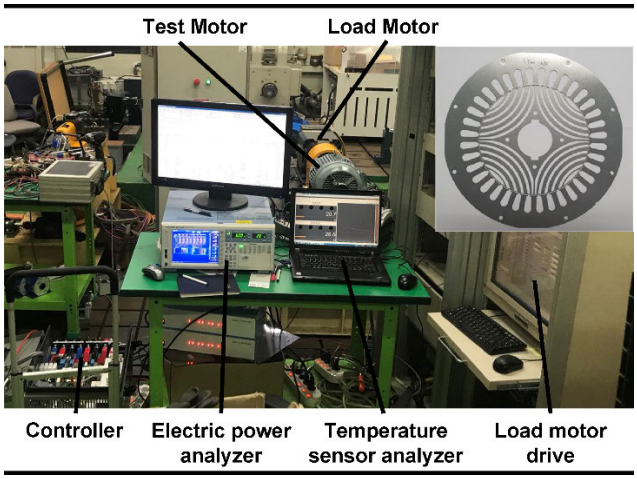

FIGURE 12. Performance test environment with the prototype.

designed based on the nonlinear MEC not only satisfies the required output but also satisfies the efficiency of IE4 (Super premium efficiency) of MEPS.

IV. CONCLUSION

This paper presents a study on the design of a high-efficiency SynRM in accordance with the MEPS. SynRMs are attracting attention as an alternative to induction motors because of their excellent manufacturability and economic advantages. However, because the structure of its rotor, composed of segments and barriers, is more complicated than that of other motors, the entire design process from basic design to optimal design depends on FEA. In this paper, the basic design method using the nonlinear MEC is proposed to simplify the basic design process for SynRM. Furthermore, the optimal design and structural analysis process using the output characteristic map according to the main design variables of the rotor for improving the output characteristics has been described. Finally, the validity of the study proposed in this paper was verified through a performance test using a prototype. The design method proposed in this paper is expected to be applicable and extendable to basic design and optimal design considering the nonlinear magnetic saturation of the stator and rotor when designing and overall motor including the SynRM.

REFERENCES

[1] A. T. de Almeida, F. J. T. E. Ferreira, and A. Q. Duarte, "Technical and economical considerations on super high-efficiency three-phase motors," *IEEE Trans. Ind. Appl.*, vol. 50, no. 2, pp. 1274–1285, Mar./Apr. 2014.

[2] *Rotating Eletrical Machines—Part 30-1 : Efficiency Classes of Line Operated AC Motors(IE-Code)*, Standard IEC60034-30-1, 2014.

[3] R. Bolter, C. U. Brunner, A. de Almeida, M. Doppelbauer, and W. Hoyt, "Eletric motor MEPS guide," Tech. Rep., 2009.

[4] H.-C. Liu and J. Lee, "Optimum design of an IE4 line-start synchronous reluctance motor considering manufacturing process loss effect," *IEEE Trans. Ind. Electron.*, vol. 65, no. 4, pp. 3104–3114, Apr. 2018.

[5] H. Kim, Y. Park, S.-T. Oh, G. Jeong, U.-J. Seo, S.-H. Won, and J. Lee, "Study on analysis and design of line-start synchronous reluctance motor considering rotor slot opening and bridges," *IEEE Trans. Magn.*, vol. 58, no. 2, pp. 1–6, Feb. 2022.

[6] K.-C. Kim, J. S. Ahn, S. H. Won, J.-P. Hong, and J. Lee, "A study on the optimal design of SynRM for the high torque and power factor," *IEEE Trans. Magn.*, vol. 43, no. 6, pp. 2543–2546, Jun. 2007.

[7] R.-R. Moghaddam and F. Gyllensten, "Novel high-performance SynRM design method: An easy approach for a complicated rotor topology," *IEEE Trans. Ind. Electron.*, vol. 61, no. 9, pp. 5058–5065, Sep. 2014.

[8] W.-H. Kim, K.-S. Kim, S.-J. Kim, D.-W. Kim, S.-C. Go, Y.-D. Chun, and J. Lee, "Optimal PM design of PMA-SynRM for wide constant-power operation and torque ripple reduction," *IEEE Trans. Magn.*, vol. 45, no. 10, pp. 4660–4663, Oct. 2009.

[9] J.-G. Lee, D.-K. Lim, and H.-K. Jung, "Analysis and design of interior permanent magnet synchronous motor using a sequential-stage magnetic equivalent circuit," *IEEE Trans. Magn.*, vol. 55, no. 10, pp. 1–4, Oct. 2019.

[10] G.-J. Park, J.-S. Kim, B. Son, and S.-Y. Jung, "Optimal design of PMa-synRM for an electric propulsion system considering wide operation range and demagnetization," *IEEE Trans. Appl. Supercond.*, vol. 28, no. 3, pp. 1–4, Apr. 2018.

[11] M. L. Bash and S. D. Pekarek, "Modeling of salient-pole wound-rotor synchronous machines for population-based design," *IEEE Trans. Energy Convers.*, vol. 26, no. 2, pp. 381–392, Jun. 2011.

[12] H. W. Derbas, J. M. Williams, A. C. Koenig, and S. D. Pekarek, "A comparison of nodal- and mesh-based magnetic equivalent circuit models," *IEEE Trans. Energy Convers.*, vol. 24, no. 2, pp. 388–396, Jun. 2009.

DONG-HOON JUNG received the B.S. degree in electrical engineering from Myongji University, Yongin, South Korea, in 2014, and the M.S. and Ph.D. degrees in electrical engineering from Hanyang University, Seoul, South Korea, in 2016 and 2020, respectively. Since 2020, he has been an Assistant Professor with the School of Mechanical, Automotive and Robot Engineering, Halla University. His research interests include design and control of electric machinery based on electro-magnetic field analysis, multi-physical design and analysis of motor/generator, energy conversion systems, and applications of motor-drives.

KI-DEOK LEE received the B.S. degree in electrical engineering from Incheon University, Incheon, South Korea, in 2009, and the M.S. and Ph.D. degrees in electrical engineering from Hanyang University, Seoul, South Korea, in 2011 and 2015, respectively. He was a Postdoctoral Student at Hanyang University, in 2015. Since 2015, he has been a Principal Research Engineer with the Korea Electronics Technology Institute, Bucheon, South Korea. His research interests include design, analysis and control of motor/generators; power conversion systems, and analysis of motors and generators. The applications are in vehicles, home appliances, and industrial electrical machinery.

JAE-KWANG LEE received the B.S. degree in electrical engineering from Kunsan National University, Kunsan, South Korea, in 2014, and the M.S. and Ph.D. degrees in electrical engineering from Hanyang University, Seoul, South Korea, in 2020. In 2020, he joined the Korea Electronics Technology Institute (KETI), where he is currently a Senior Researcher with the Intelligent Mechatronics Research Center. His research interests include design of electric machinery, analysis, testing and control of motor/generator; power conversion systems, and applications of motor drives.